Title

FATIGUE CRACK PROPAGATION IN ALUMINUM-LITHIUM ALLOY 2090: PART II. SMALL CRACK BEHAVIOR

Authors

Rao, K.T. Venkateswara
Yu, W.
Ritchie, R.O.

Publication Date

1986-11-01

LBL-22179
Preprint

Lawrence Berkeley Laboratory
UNIVERSITY OF CALIFORNIA

Materials & Chemical Sciences Division

Center for Advanced Materials

Submitted to Metallurgical Transactions A

FATIGUE CRACK PROPAGATION IN ALUMINUM-LITHIUM ALLOY 2090: PART II. SMALL CRACK BEHAVIOR

K.T. Venkateswara Rao, W. Yu, and R.O. Ritchie

November 1986

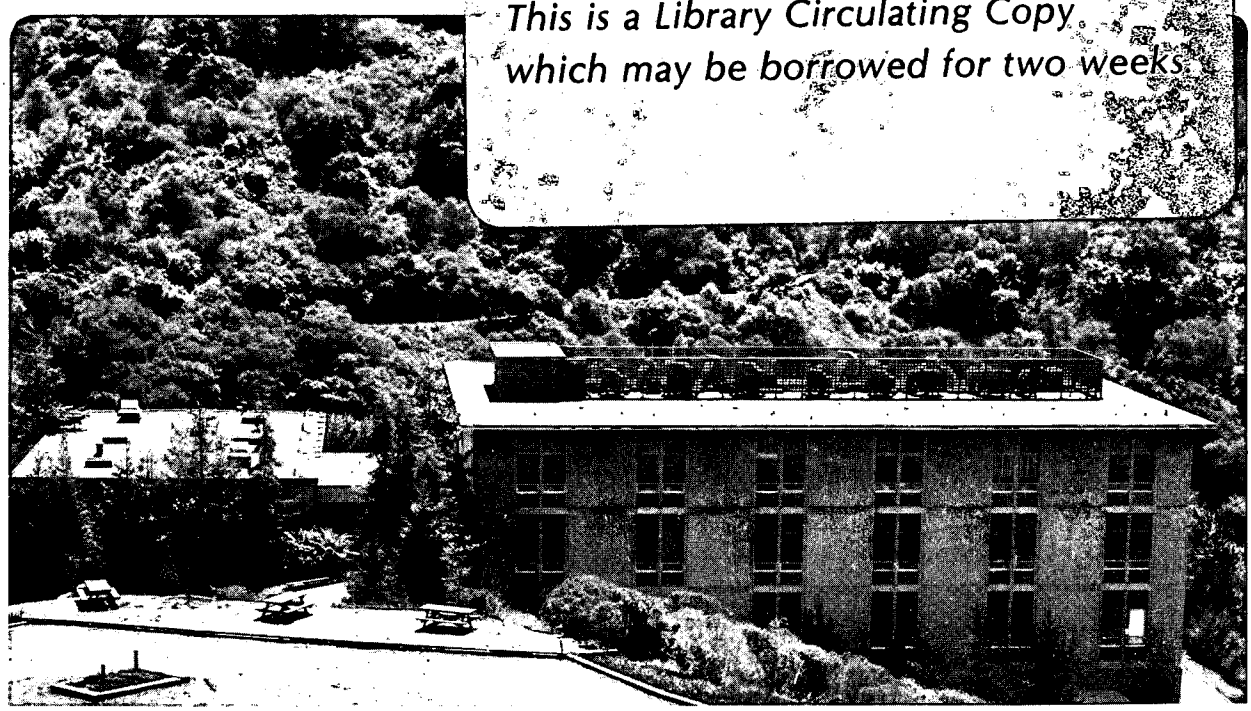

Prepared for the U.S. Department of Energy under Contract DE-AC03-76SF00098

DISCLAIMER

LBL-22179

FATIGUE CRACK PROPAGATION IN ALUMINUM-LITHIUM ALLOY 2090:

PART II. SMALL CRACK BEHAVIOR

K. T. Venkateswara Rao, W. Yu and R. O. Ritchie

Center for Advanced Materials, Lawrence Berkeley Laboratory, and
Department of Materials Science and Mineral Engineering,
University of California, Berkeley, CA 94720

November 1986

submitted to Metallurgical Transactions A

This work was supported by the Director, Office of Energy Research, Office of Basic Energy Sciences, Materials Sciences Division of the U.S. Department of Energy under Contract No. DE-AC03-76SF00098.

FATIGUE CRACK PROPAGATION IN ALUMINUM-LITHIUM ALLOY 2090:

PART II. SMALL CRACK BEHAVIOR

K. T. Venkateswara Rao, W. Yu and R. O. Ritchie

Center for Advanced Materials, Lawrence Berkeley Laboratory, and
Department of Materials Science and Mineral Engineering,
University of California, Berkeley, CA 94720

ABSTRACT

A study has been made of the mechanics and mechanisms of fatigue crack propagation in a commercial plate of aluminum-lithium alloy 2090-T8E41. In Part II, the crack growth behavior of naturally-occurring, microstructurally-small (2 to 1000 μm) surface cracks is examined as a function of plate orientation, and results compared with those determined in Part I on conventional long ($\gtrsim$ 5 mm) crack samples. It is found that the near-threshold growth rates of small cracks are between 1 to 3 orders of magnitude faster than those for long cracks, subjected to the same nominal stress intensity ranges (at a load ratio of 0.1). Moreover, the small cracks show no evidence of an intrinsic threshold and propagate at ΔK levels as low as 0.7 MPa$\sqrt{m}$, far below the long crack threshold ΔK_{TH}. Their behavior is also relatively independent of orientation. Such accelerated small crack behavior is attributed primarily to restrictions in the development of crack tip shielding (principally from roughness-induced crack closure) with cracks of limited wake. This notion is supported by the close correspondence of small crack results with long crack growth rates plotted in terms of ΔK_{eff} (i.e., after allowing for closure above the effective long crack threshold). Additional factors, including the different statistical sampling effect of large and small cracks with microstructural features, are briefly discussed.

K. T. VENKATESWARA RAO, W. YU and R. O. RITCHIE are Graduate Student, Research Engineer, and Professor, respectively, with the Center for Advanced Materials, Lawrence Berkeley Laboratory, and the Department of Materials Science and Mineral Engineering, University of California, Berkeley, CA 94720.

I. INTRODUCTION

Damage-tolerant design concepts, currently in use to ensure the durability of both military and civil aircraft, generally specify that small ($\sim$ 100 μm) corner cracks be assumed to pre-exist at each fastener hole in the structure (e.g., ref. 1). Lifetime is then computed in terms of the time, or number of fatigue cycles, for any one of these cracks to propagate to critical size, based on the integration, from initial to final defect size, of a relationship describing the crack growth rates as function of the mechanical "crack driving force" (e.g., the stress intensity range, ΔK) for the material in question. Such crack growth relationships are generally derived from data measured on laboratory specimens containing crack sizes in excess of 5 to 10 mm.

However, in recent years it has become apparent that where cracks are physically small (i.e., $\lesssim$ 1 mm), or where they approach the size-scales of the microstructure or the extent of local plasticity, their growth rate behavior may not conform to that measured conventionally with long ($\gtrsim$ 5 mm) cracks (2-21). In fact as illustrated schematically in Fig. 1, small crack growth rates are generally non-unique and can markedly exceed those of long cracks when subjected to the same nominal "crack driving force", e.g., at

the same ΔK (2-9).* Such apparently anomalous behavior is most

*Similar anomalous behavior has been reported for so-called "chemically small" cracks, where differences in the **local** crack tip environment (controlled by frequency and reaction kinetics) can cause small cracks to propagate at rates some 1.5 to several hundred times faster than long cracks at the same mechanical "driving force" (6,22).

prevalent at low load ratios in the low growth rate ($\lesssim 10^{-9}$ m/cycle) near-threshold regime (except for flaws emanating from notches (4,11)), where specifically small cracks have been observed to propagate at stress intensity ranges **below** the fatigue threshold, ΔK_{TH}, at which long crack growth becomes dormant (e.g., refs. 5,8). The problem is of practical significance as damage-tolerant calculations are invariably based on long crack data, and depending upon initial flaw size, overall life is generally dominated by the regime where the crack is both small and advancing at low growth rates. Consequently, with the accelerated near- and sub-threshold growth rate behavior of small cracks, there exists a potential for dangerously non-conservative predictions of life (5).

There are several origins of the lack of similitude between long and small crack growth behavior (2-9). These are summarized in Table I, which is taken from ref. 8. Where cracks are comparable in size with the crack tip plastic zone, or are embedded within the strain field of a notch ("mechanically-small"), differences may result from an inappropriate use of linear elastic fracture mechanics, specifically the stress intensity, in characterizing crack tip

fields. Conversely, for microstructurally-small cracks, differences can arise from an inappropriate use of continuum mechanics to describe the preferential initiation and growth of naturally-occurring flaws, of a size comparable with microstructural features, at local inhomogeneities within the microstructure. Other major distinctions may involve the initial non-uniform growth of small (surface) flaws (13,14), enhanced cyclic plastic strains at the tips of microstructurally-small cracks (12), differing interactions with grain or phase boundaries (15,16), and environmental effects (6,22).

Table I. Classes of Small Cracks (8)

Type of Small Crack	Dimension	Responsible Mechanism	Potential Solution
Mechanically-small	$a \lesssim r_y$ †	excessive (active) plasticity	use of ΔJ, ΔS $\Delta CTOD$
Microstructurally-small	$a \lesssim d_g$ †† $2c \lesssim 5\text{-}10\ d_g$	crack tip shielding enhanced $\Delta\varepsilon_p$ crack shape	probabilistic approach
Physically-small	$a \lesssim 1$ mm	crack tip shielding (crack closure)	use of ΔK_{eff}
Chemically-small	up to 10 mm#	local crack tip environment	

†r_y is plastic zone size or plastic field of notch.

††d_g is critical microstructural dimension, e.g., grain size, a is the crack depth and 2c the surface length.

#Critical Size is a function of frequency and reaction kinetics.

However, in essence the problem is one of defining an appropriate "crack driving force" for small crack growth, which accounts for excessive plasticity ahead of the crack tip and more importantly crack tip shielding behind it (17).

The role of crack tip shielding, which results from mechanisms which reduce the **local** "crack driving force", is central to the issue of the "anomalous" behavior of small flaws, as shielding mechanisms primarily act on the crack wake and thus can induce crack size dependent behavior (17,23). Small cracks, by virtue of their limited wake, are less able to develop the same magnitude of shielding as equivalent long cracks at the same nominal ΔK, and thus experience a larger **local** "driving force" (3,5,10,11,14,17). This notion is supported by experiments which show the development of crack closure with the initial extension of small cracks (14,17-20), and the closer normalization of long and small crack growth rates when plotted as a function of ΔK_{eff}, i.e., in terms of characterizing parameters which at least partially account for shielding (11,21).

Such considerations are of particular significance to aluminum-lithium alloys, since they derive their superior crack growth resistance primarily from crack tip shielding (17,23) mechanisms. As described in Part I of this paper (24), the marked planar slip characteristics and anisotropic nature of the microstructures in Al-Li-X alloys, such as 2090, confer excellent long crack fatigue properties, primarily from the generation of strongly crystallographic and meandering crack paths. This in turn promotes

significant shielding from crack deflection and consequent (roughness-induced) crack closure induced by the wedging of fracture surface asperities (24-28). Thus, in view of this reliance on shielding mechanisms, it might be anticipated that under conditions where such shielding is restricted, such as with cracks of limited wake, the superior crack growth properties may be compromised. Accordingly, discrepancies between long and small crack behavior in these alloys may be expected to be large.

It is thus the objective of Part II of this paper to examine the propagation behavior of naturally-occurring, microstructurally-small (2 to 1000 μm) surface cracks in the Al-Li-Cu-Zr alloy 2090-T8E41, as a function of plate orientation, and to compare results with those measured on conventional long ($\gtrsim$ 5 mm) crack samples in Part I (24).

II. EXPERIMENTAL PROCEDURES

The material studied was a 12.7 mm thick plate of commercial Al-Li-Cu-Zr alloy 2090, supplied by ALCOA in the near peak-aged and thermomechanically treated T8E41 condition. A description of the composition, heat treatment, microstructure and mechanical properties is given in Part I of this paper (24).

Tests to examine the fatigue crack propagation behavior of naturally-occurring, microstructurally-small surface cracks were performed on 7.6 mm thick, unnotched, rectangular four-point bend specimens, machined in the T-L, L-T and T-S orientations (Fig. 2).

At least six tests were conducted for each orientation. The geometry of the bend samples was waisted, specifically for the T-S orientation, to minimize the possibility of delamination along the length of the specimen, perpendicular to the short-transverse direction. Tests were carried out in controlled room temperature air ($22^{o}C$, 45% relative humidity) at a load ratio ($R = K_{max}/K_{min}$) of 0.1 and a sinusoidal frequency of 50 Hz.

To initiate cracking, maximum tensile stresses on the top surface of the specimen were approximately 0.9 times the yield stress of the material. Crack initiation and growth on this surface, which had previously been electropolished, were monitored by means of cellulose acetate replicas. Tests were periodically interrupted and held at mean load during replication. Replicas were subsequently gold coated by sputtering, to permit better resolution of the surface crack length (2c), and examined using optical microscopy. With such procedures, small cracks of lengths between 2 and 1000 μm could be readily monitored.

Owing to crack branching, surface crack lengths were taken as the projected crack length normal to the direction of the tensile bending stresses. An a/c ratio (half the surface crack length to the crack depth) of 0.8 was assumed, based on studies of crack geometry using serial sectioning of various surface flaws. Stress intensity factors for such flaws were computed using the Newman and Raju linear elastic solution for semi-elliptical surface flaws (29). Data are presented in terms of the nominal stress intensity range, given by ΔK

= K_{max} - K_{min}. Use of the stress intensity to characterize small crack growth was deemed to be appropriate in the present work, as computed maximum and cyclic plastic zone sizes remained small (0.4 to 150 μm and 0.1 to 30 μm, respectively) compared to specimen dimensions.

Small crack growth rates were compared with long ($\gtrsim$ 5 mm) crack results, measured on pre-existing through-thickness cracks in compact C(T) and single-edge-notched bend SEN(B) samples, as described in Part I (24). Long crack data were presented in terms of the nominal and effective stress intensity ranges, the latter being defined as $\Delta K_{eff} = K_{max} - K_{cl}$, where K_{cl} is the closure stress intensity, measured at first contact of the fracture surfaces during unloading, using back-face strain compliance techniques (17).

III. RESULTS AND DISCUSSION

The fatigue crack growth behavior of microstructurally-small (2 to 1000 μm) surface cracks in the L-T, T-L and T-S orientations are plotted as a function of the crack length (i.e., depth of surface flaw) in Fig. 3. Cracks as small as 2 μm show growth rates exceeding 10^{-10} m/cycle, with little apparent effect of plate orientation. The extensive scatter can be considered to be inherent in the growth rate behavior of naturally-occurring small flaws, as they initiate and grow within a few favorably oriented grains and then suffer local

impedence as they encounter microstructural features such as grain or phase boundaries.

Fractographically, small crack initiation was generally seen to be associated with inclusions or intermetallic particles. Corresponding crack path morphologies for small crack growth in the three orientations are shown in the three-dimensional micrograph in Fig. 4. Cracks in the L-T orientation were consistently inclined at 30^{o} to the tensile axis, presumably due to the strong texture in the alloy. They appeared remarkably linear, without microscopic deflection, consistent with a relatively flat fracture surface topography in scanning electron fractographs (Fig. 5a). Crack paths in the T-L and T-S orientations, conversely, were locally deflected, which resulted in coarser, more faceted fracture surface morphologies (Fig. 5b). The nature of this deflection appeared to be crystallographic and involved extensive slip band cracking (Fig. 6).

Comparison of the small crack growth rate data in the three orientations with that measured at R = 0.1 for long cracks (24) is shown in Fig. 7 as a function of the nominal ΔK. It is apparent that, whereas the growth rates of long and small cracks are comparable at higher ΔK levels typically above $\sim$ 8 MPa$\sqrt{m}$, the near-threshold propagation rates of small flaws are between 1 to 3 orders of magnitude faster than those for long flaws, subjected to the same nominal ΔK. Moreover, small crack growth can be seen at ΔK levels as low as 0.7 MPa$\sqrt{m}$, far below the long crack threshold ΔK_{TH}.

The primary reason for such marked discrepancies in long and small crack growth rates at near-threshold levels can be readily appreciated by replotting the long crack data in terms of ΔK_{eff}, after allowing for crack closure (i.e., by utilizing the back-face strain measurements of K_{cl} in Part I (24). As shown in Fig. 7, it is apparent that the scatter bands for small crack growth rates now come into close correspondence with long crack results, indicating that their accelerated behavior results primarily from reduced shielding. This clearly implies a critical role of crack tip shielding during fatigue crack growth in aluminum-lithium alloys both in promoting superior long crack resistance (24-28) and, when restricted with cracks of limited wake, in causing significantly enhanced small crack growth rates. Similar effects of reduced crack growth resistance from reductions in shielding have been reported for the 2090 alloy following periodic compression overloads (28). With increasing crack size, however, K_{cl} values gradually approach saturation long crack values, such that the small crack growth rates merge with long crack results. This is shown in Fig. 7 for nominal ΔK levels above roughly 10 MPa$\sqrt{m}$. Moreover, at the higher stress intensity ranges, the role of wedge shielding mechanisms, such as roughness-induced closure, become diminished even for long cracks, due to the larger crack opening displacements (30).

Although the reduced role of crack closure at small crack sizes appears to be the major reason for their accelerated growth rate behavior, it is apparent from Fig. 7 that the smallest cracks, e.g.,

typically of a length less than 5 μm, show no indications of an intrinsic threshold. Moreover, **they continue to grow at ΔK levels as low as 0.7 MPa$\sqrt{m}$, well below the long crack ΔK_{eff} threshold** (i.e., after correcting for closure), implying that other factors are pertinent. One such difference may be related to experimental evidence that suggests that small flaws may experience higher cyclic plastic strains at their tips (12). However, a more important effect may be associated with differences in the statistical sampling of microstructural features encountered by large and small cracks (8). For example, the naturally-occurring small surface crack will tend to initiate at preferred "soft spots" in the microstructure and, unlike pre-existing long through-thickness cracks, will not have its growth averaged over many disadvantageously oriented grains, since its crack front will encompass only a few grains. Furthermore, the microstructurally-small crack, which corresponds to a three-dimensional flaw whose plastic zone is typically smaller than the key microstructural dimension, such as grain size, will advance as if in a single crystal, preferentially oriented for operation of the relevant crack extension mechanism.

Clearly, in such cases, where crack sizes are below any continuum approximation, it is inappropriate to talk of an intrinsic threshold for crack propagation which can be described in terms of a continuum parameter such as the stress intensity. In fact, where damage tolerant design and lifetime calculations are extended to crack sizes of such microstructural dimensions, characterization

using deterministic methods in general must eventually become questionable, and ideally should be replaced by probabilistic methodologies.

IV. CONCLUDING REMARKS

From a perspective of summarizing the fatigue crack propagation resistance of aluminum-lithium alloy 2090-T8E41 (as 12.7 mm thick plate), it is clear that the superior long crack growth properties (compared to traditional high strength aluminum alloys) and the anomalously high small crack growth rates paradoxically are a consequence of the same phenomenon, namely significant crack tip shielding from crack deflection and particularly roughness-induced crack closure, resulting from highly deflected and meandering crack paths. Characteristic of the "extrinsic toughening" approach (17,23), such mechanisms are extremely potent in impeding crack advance, particularly at low applied "driving forces", yet are largely irrelevant for crack initiation resistance and are far less effective in impeding the growth of small cracks with limited wake. However, where the shielding can remain active, such as with the growth of long cracks under constant amplitude and especially tension-dominated variable amplitude loading conditions, the peak aged 2090 alloy shows a remarkable combination of high strength and fatigue crack growth resistance. Conversely, for the initial growth of small fatigue cracks, from fastener holes for example, which can

often provide the major contribution to overall fatigue life, the 2090 alloy is less attractive.

Finally, it should be noted that the crack deflection and branching originates not simply from the marked planar slip characteristics of 2090-T8E41 but also from the highly textured nature of the alloy. Thus, although long crack growth rates are much faster (and the fracture toughness much lower) perpendicular to the short-transverse direction (i.e., in the rolling plane), it is the tendency for delamination in this direction which actually helps promote shielding and hence the beneficial crack growth properties in the longitudinal and transverse orientations. Accordingly, although future improvements in the short-transverse properties of aluminum-lithium alloys, through refinements in chemistry and processing, may significantly enhance the short-transverse toughness and small crack growth resistance, such procedures may actually compromise the superior long crack fracture and fatigue properties in the other orientations.

V. CONCLUSIONS

Based on a comparison of the fatigue crack propagation behavior (at $R = 0.1$) of pre-existing long ($\gtrsim$ 5 mm) through-thickness cracks and naturally-occurring microstructurally-small (2 to 1000 μm) surface cracks in the L-T, T-L and T-S orientations of a 12.7 mm

thick plate of commercial Al-Li-Cu-Zr alloy 2090-T8E41, the following conclusions can be made:

1. The near-threshold fatigue crack propagation rates of small flaws were found to exceed those of long cracks by 1 to 3 orders of magnitude at the same nominal ΔK levels. Small crack growth rates, which appeared to be relatively insensitive to plate orientation, were observed to proceed at ΔK levels as low as 0.7 MPa$\sqrt{m}$, well below the fatigue threshold stress intensity range, ΔK_{TH}, where long cracks become dormant.

2. Whereas long crack growth behavior is characterized by extensive crack tip shielding from crack deflection and resulting roughness-induced crack closure from branched crystallographic crack paths, the restriction of such closure with small cracks of limited wake appears to be the primary reason for their accelerated growth. This notion is supported by the close correspondence of small crack data with long crack results expressed in terms of ΔK_{eff}, i.e., after correcting for closure.

3. Unlike long cracks, small crack growth rates show no signs of an intrinsic threshold and continue to propagate at stress intensity levels below the closure-corrected ΔK_{eff} long crack threshold. This suggests that factors other than shielding may be additionally involved, such as the enhanced cyclic plastic strains at the tips of small cracks and the differing statistical sampling effect of large and small cracks with microstructural features.

4. Finally, it is concluded that the superior long crack growth rates and the anomalously high small crack growth rates in this alloy are primarily a consequence of the same phenomenon, i.e., a marked dependence on extrinsic "toughening" mechanisms, primarily from crack meandering and resulting crack closure. Although crack tip shielding provides a potent impedence mechanism for long crack growth, it cannot similarly remain effective for cracks of limited wake.

ACKNOWLEDGEMENTS

This work was supported by the Director, Office of Energy Research, Office of Basic Energy Sciences, Materials Sciences Division of the U.S. Department of Energy under Contract No. DE-AC03-76SF00098, under the auspices of the Center for Advanced Materials. Thanks are due to Drs. P. E. Bretz, R. J. Bucci and R. R. Sawtell of ALCOA for helpful discussions and provision of the 2090 plate, to D. Fenwick, L. Gill and L. Rumaner for experimental assistance, and to Ms. M. Penton for help in preparing the manuscript.

REFERENCES

1. Anon: "Airplane Damage Tolerance Requirements", Military Specification MIL-A-83444, United States Air Force, July 1974.

2. S. J. Hudak: J. Eng. Matls. Tech., Trans ASME, Series H, vol. 103, 1981, pp. 26-35.

3. J. Schijve: in Fatigue Thresholds, J. Bäcklund, A. F. Blom, and C. J. Beevers, eds., EMAS Ltd., Warley, U.K., vol. 2, 1982, pp. 881-908.

4. K. J. Miller: Fat. Eng. Mat. Struct., vol. 5, 1982, pp. 223-32.

5. S. Suresh and R. O. Ritchie: Int. Metals Reviews, vol. 29, 1984, pp. 445-76.

6. R. P. Gangloff and R. O. Ritchie: in Fundamentals of Deformation and Fracture, B. A. Bilby, K. J. Miller, and J. R. Willis, eds., Cambridge University Press, Cambridge, U.K., 1985, pp. 529-58.

7. J. Lankford: Fat. Fract. Eng. Mat. Struct., vol. 8, 1983, pp. 161-75.

8. R. O. Ritchie and J. Lankford: Mater. Sci. Eng., vol. 84, 1986, pp. 11-6.

9. R. O. Ritchie and J. Lankford, eds.: "Small Fatigue Cracks", TMS-AIME, Warrendale, PA, 1986.

10. J. F. McCarver and R. O. Ritchie: Mater. Sci. Eng., vol. 55, 1982, pp. 63-7.

11. K. Tanaka and Y. Nakai: Fat. Eng. Mat. Struct., vol 6, 1983, pp. 315-27.

12. J. Lankford and D. L. Davidson: in ref. 9, pp. 51-71.

13. L. Wagner, J. K. Gregory, A. Gysler, and G. Lütjering: in ref. 9, pp. 117-28.

14. A. Pineau: in ref. 9, pp. 191-211.

15. M. R. James and W. L. Morris: in ref. 9, pp. 145-56.

16. K. Tanaka: in ref. 9, pp. 343-61.

17. R. O. Ritchie and W. Yu: in ref. 9, pp. 167-89.

18. F. Heubaum and M. E. Fine: Scripta Met., vol. 18, 1984, pp. 1235-40.

19. K. Minakawa, H. Nakamura, and A. J. McEvily: ibid., pp. 1371-4.

20. E. Zaiken and R. O. Ritchie: Metall. Trans. A, vol. 16A, 1985, pp. 1467-77.

21. K. T. Venkateswara Rao, W. Yu, and R. O. Ritchie: Scripta Met., vol. 20, 1986, pp. 1459-65.

22. R. P. Gangloff and R. P. Wei: in ref. 9, pp. 239-64.

23. R. O. Ritchie and R. M. Cannon: "Crack Tip Shielding in Fracture and Fatigue: Extrinsic vs. Intrinsic Toughening", Lawrence Berkeley Laboratory Report No. LBL-20656, University of California, Berkeley, 1986.

24. K. T. Venkateswara Rao, W. Yu, and R. O. Ritchie: Part I, submitted to Metall. Trans. A, vol. 18A, 1987.

25. J. Petit, S. Suresh, A. K. Vasudévan, and R. C. Malcolm: in Aluminium-Lithium Alloys III, C. Baker, P. J. Gregson, S. J. Harris, and C. J. Peel, eds., Institute of Metals, London, U.K., 1986 pp. 257-62.

26. K. V. Jata and E. A. Starke: ibid., pp. 247-56.

27. M. Peters, K. Welpmann, W. Zink, and T. H. Sanders: ibid., pp. 239-46.

28. W. Yu and R. O. Ritchie: J. Eng. Matls. Tech., Trans. ASME, Series H, Vol. 109, 1987.

29. J. C. Newman, Jr. and I. S. Raju: Eng. Fract. Mech., vol. 15, 1981, pp. 185-92.

30. S. Suresh and R. O. Ritchie: in Fatigue Crack Growth Threshold Concepts, D. L. Davidson and S. Suresh, eds., TMS-AIME, Warrendale, PA, pp. 227-61.

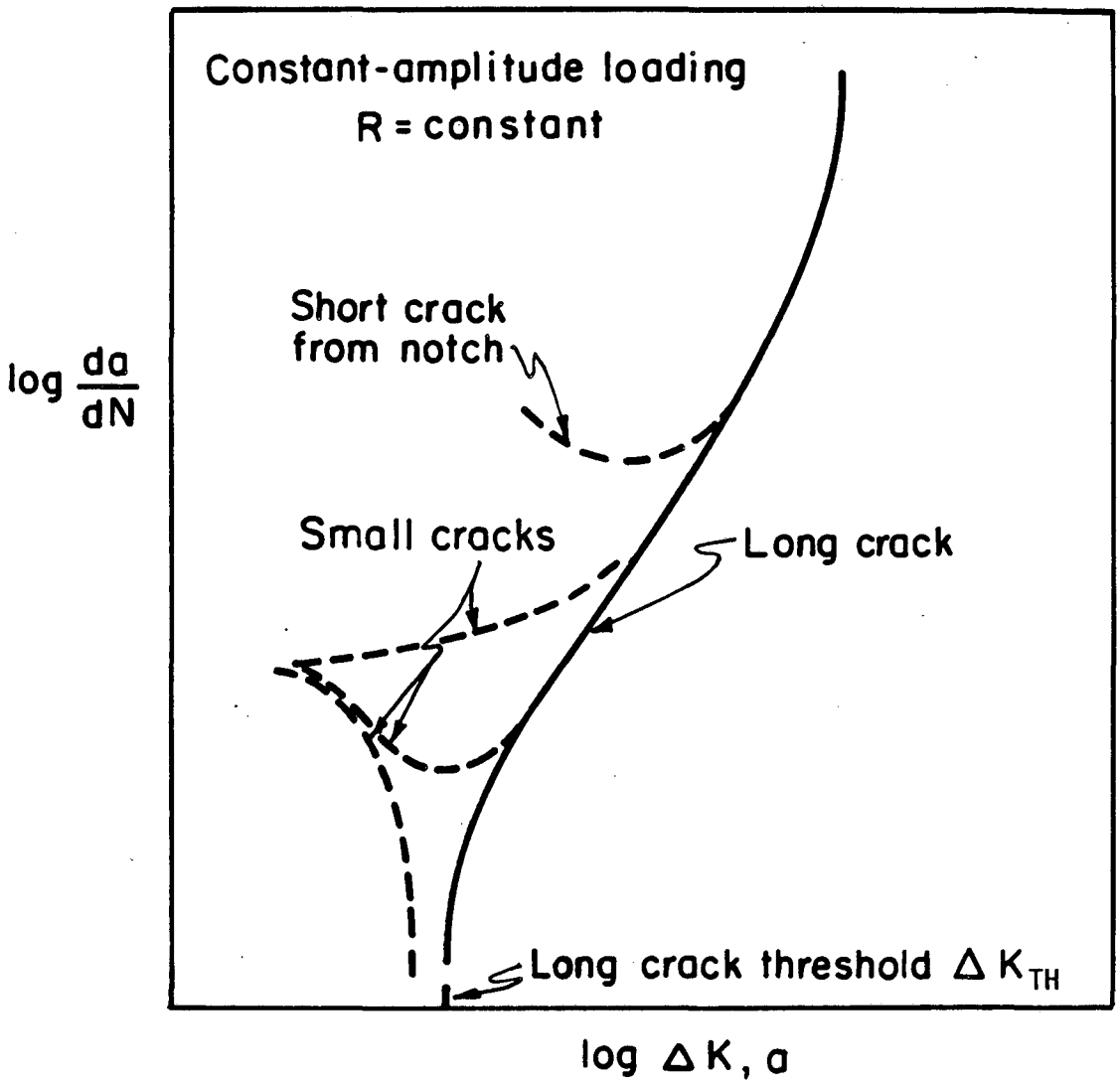

XBL 835-9687 A

Fig. 1: Schematic representation of the typical variation in fatigue crack growth rates da/dN, with nominal stress intensity range ΔK, or crack length a, for "long" and "small" cracks. ΔK_{TH} is the nominal fatigue threshold stress intensity range, below which long cracks remain dormant.

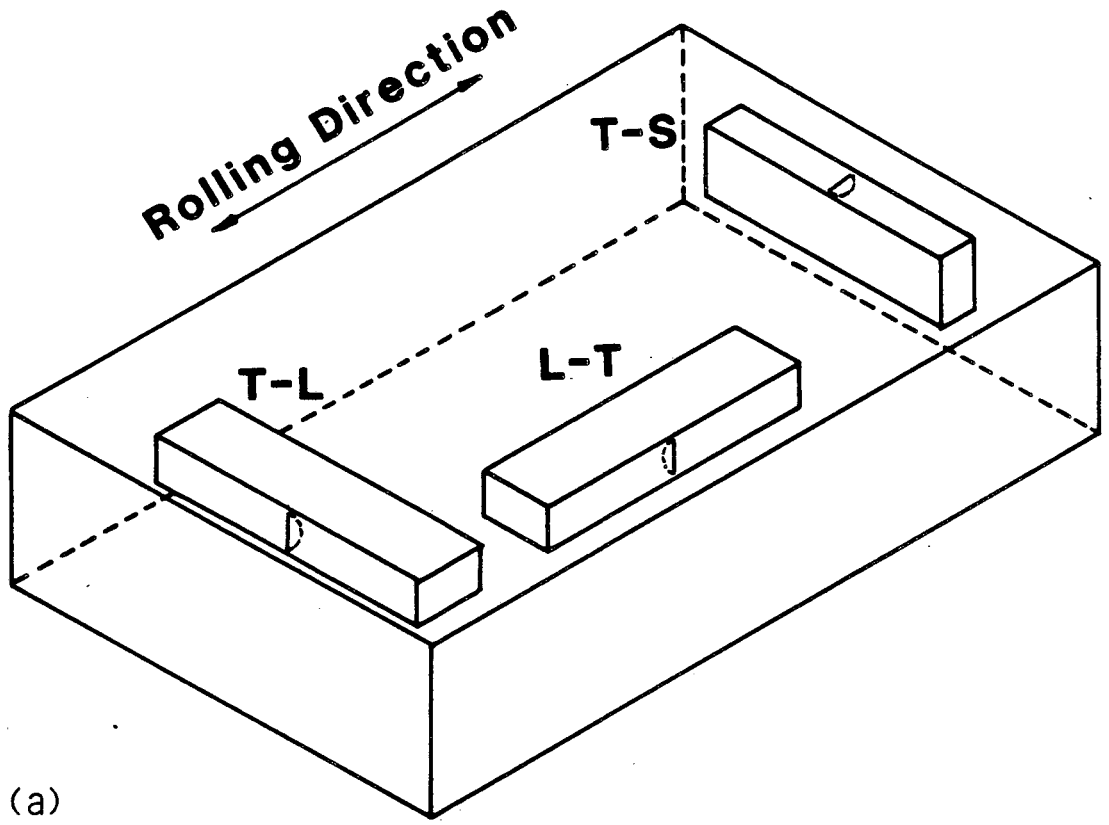

Fig. 2: a) Plate orientation and b) geometry of test specimens used to measure small crack growth behavior in the 2090-T8E41 alloy.

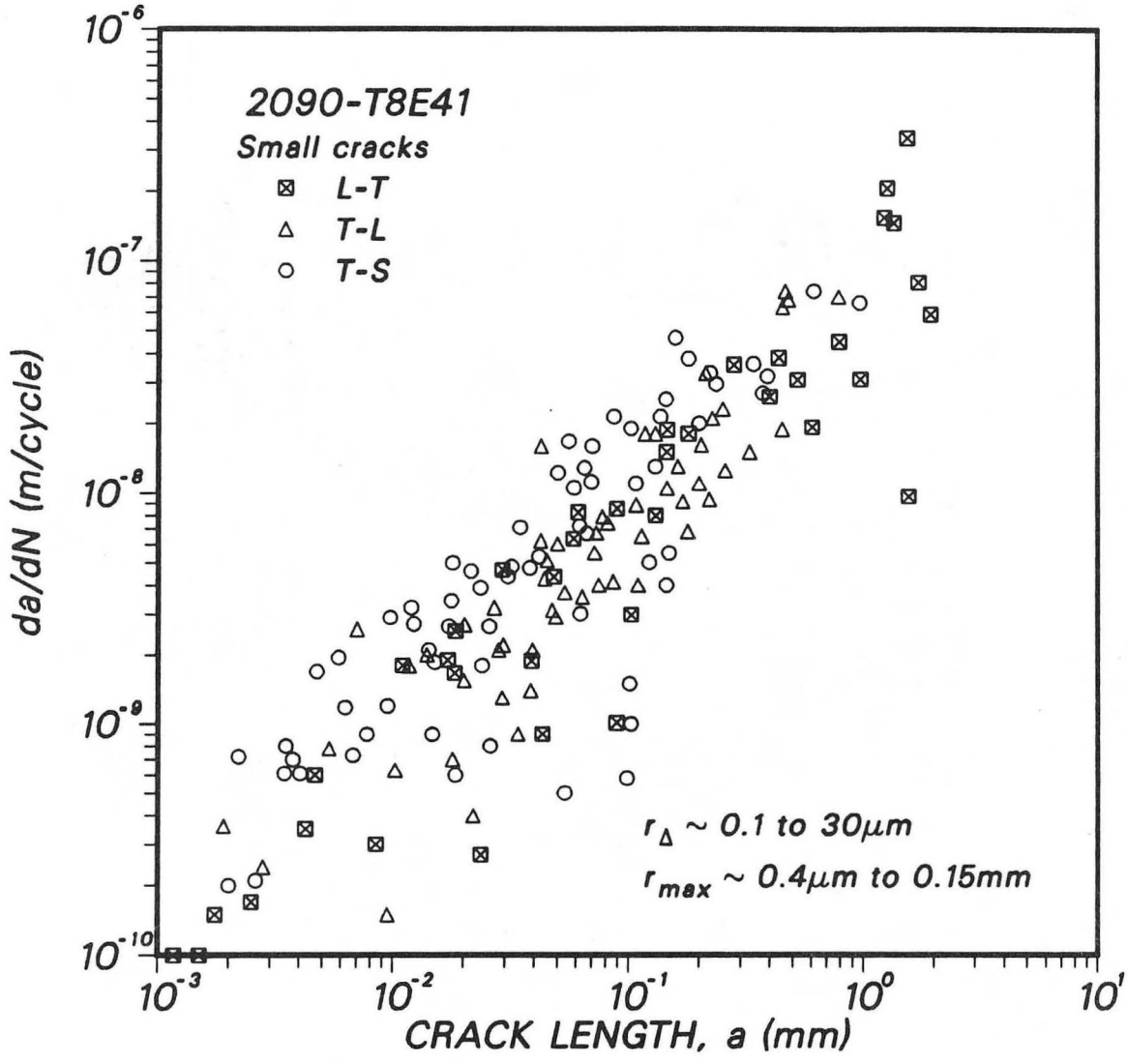

XBL 8610-3624

Fig. 3: Variation in the growth rates, da/dN, of small (2 to 1000 μm) surface fatigue cracks in peak-aged 2090-T8E41 alloy as a function of crack depth, a. Data are presented at R = 0.1 for the L-T, T-L and T-S orientations, based on replication measurements on SEN(B) specimens.

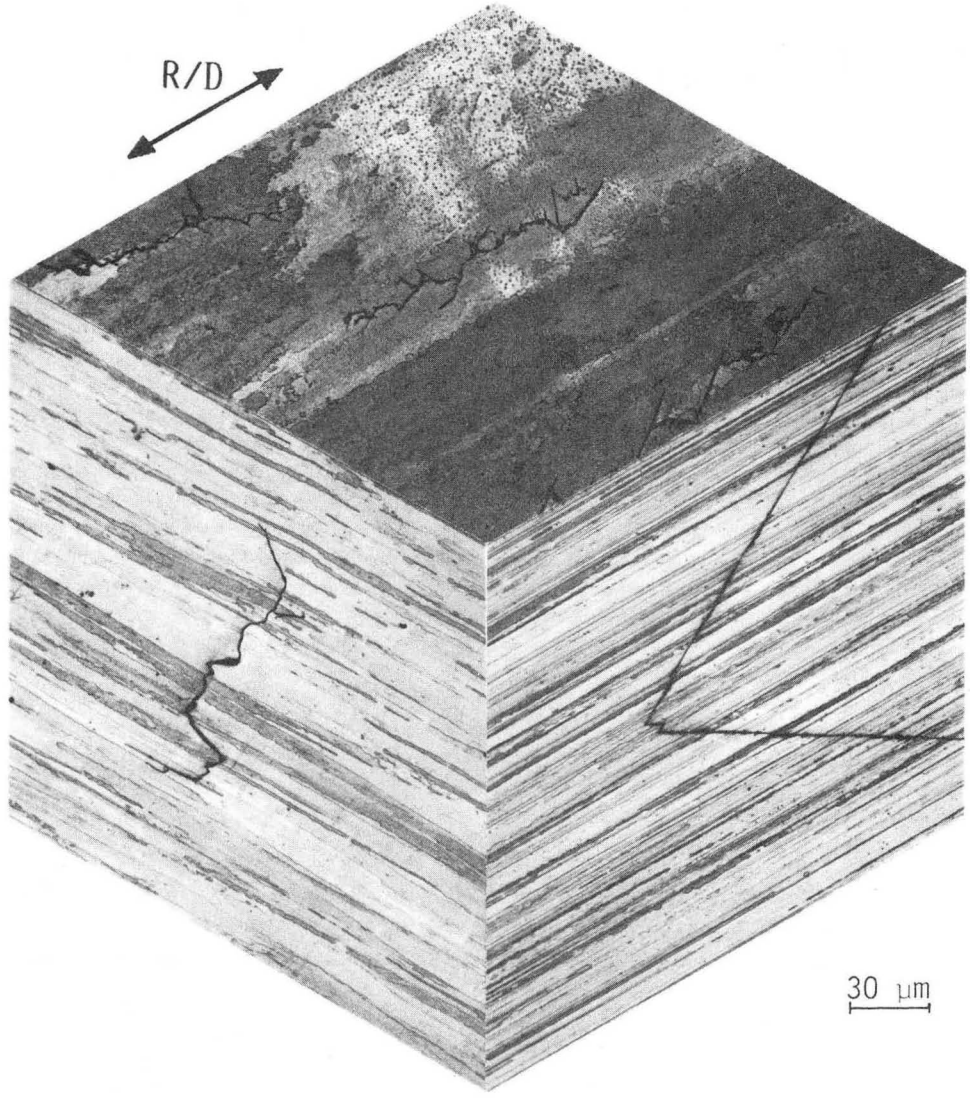

XBB 869-7357

Fig. 4: Three-dimensional optical micrograph showing the morphology of the surface crack path of small fatigue cracks in the L-T, T-L and T-S orientations in 2090-T8E41 alloy (Keller's reagent etch).

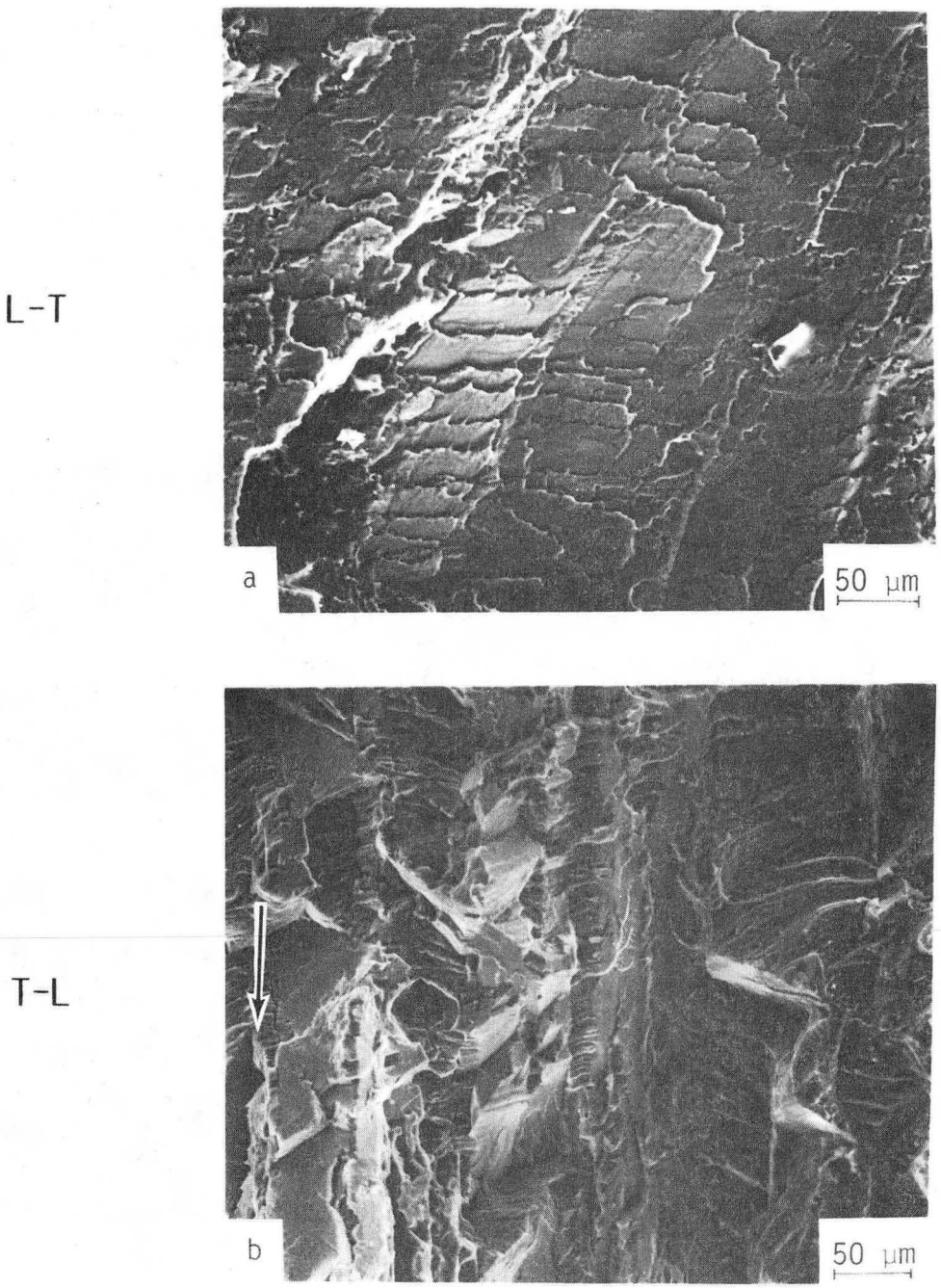

Fig. 5: Fractography of small crack growth in 2090-T8E41 in a) L-T, and b) T-L orientations. Arrow indicates general direction of crack advance.

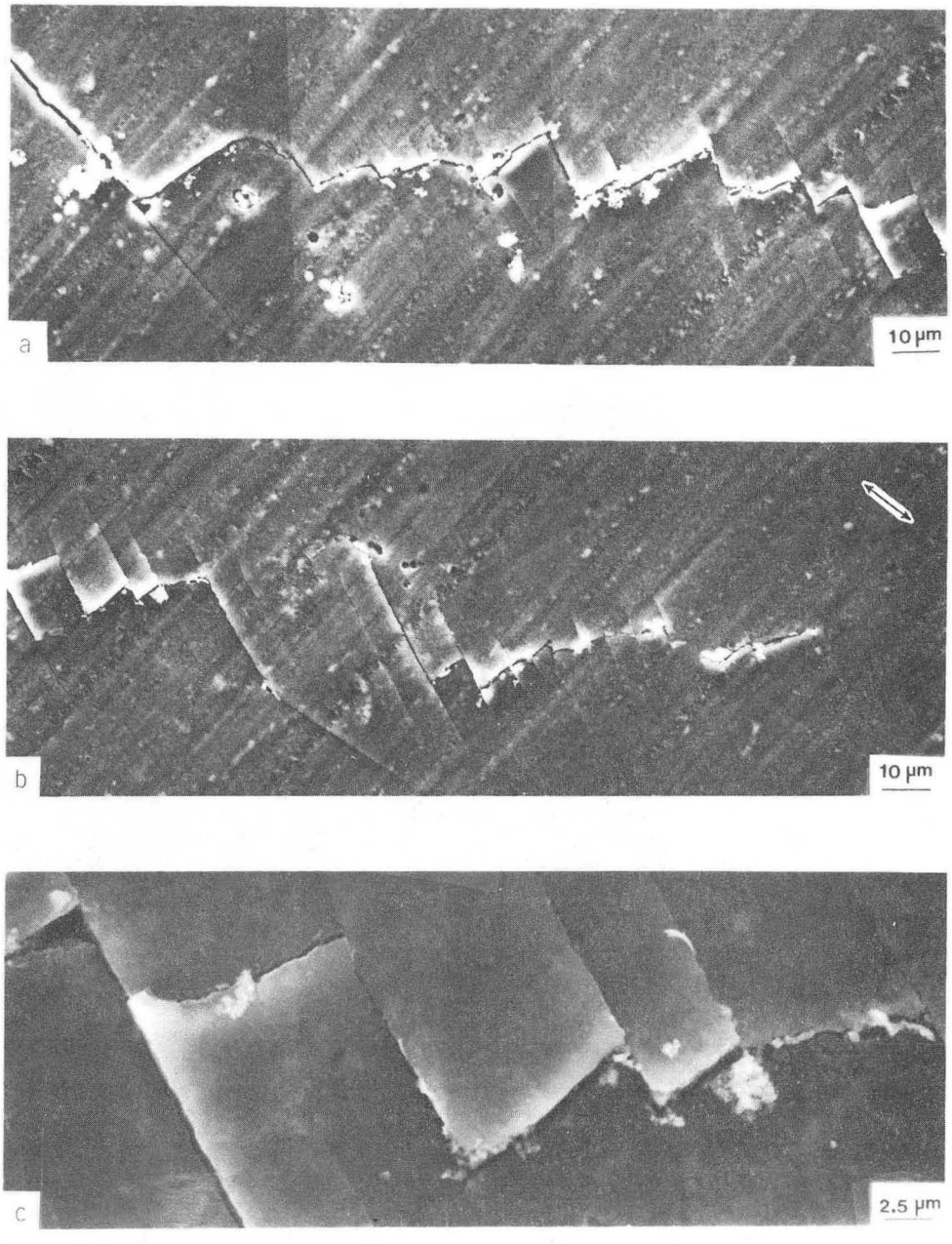

XBB 868-6195

Fig. 6: Scanning electron micrographs showing the crack path morphology of small crack extension in the T-S orientation, involving extensive slip-band cracking. Arrow indicates the direction of the stress axis.

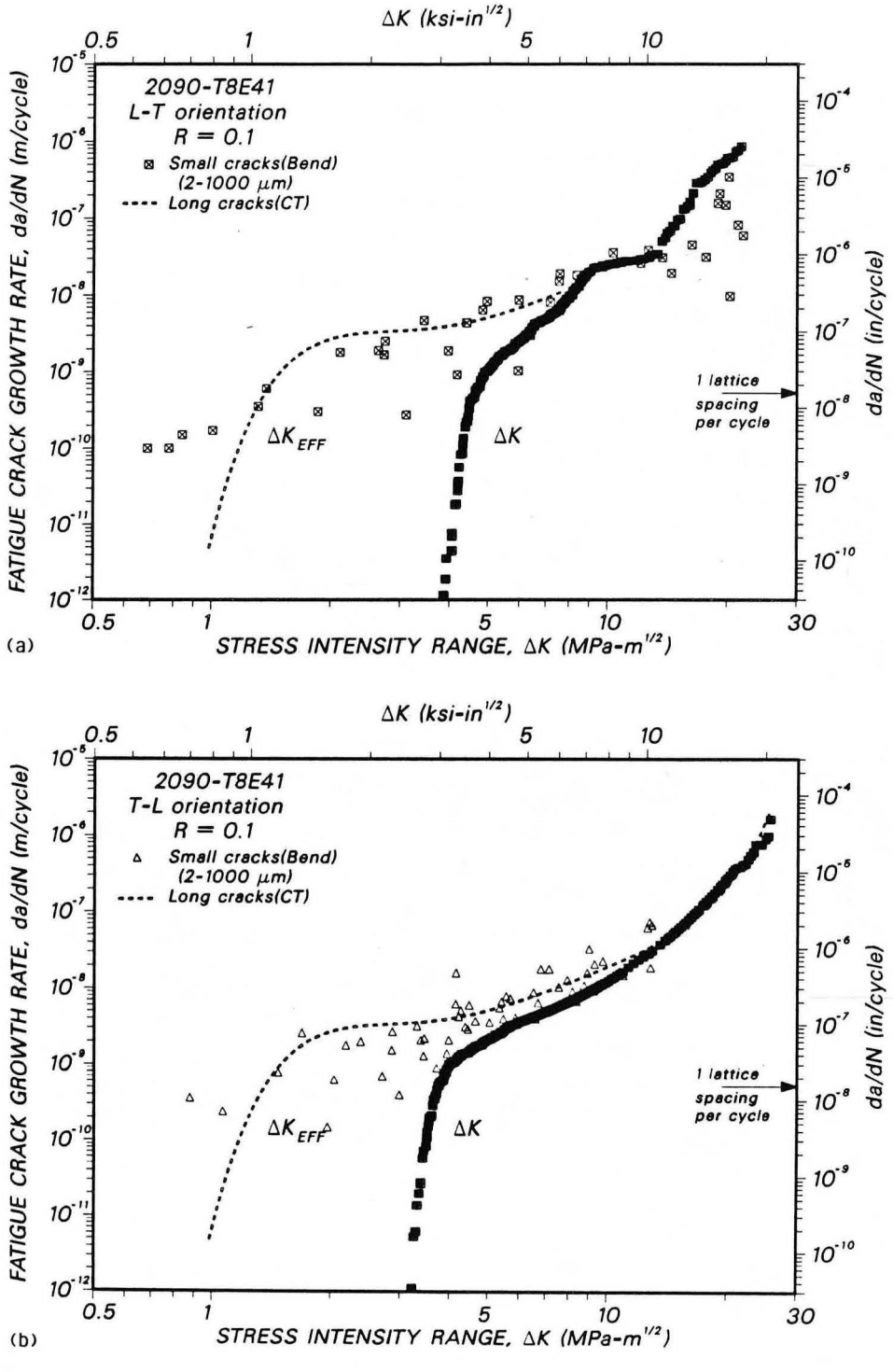

Fig. 7: Comparison of the growth rates of long (≳ 5 mm) and microstructurally-small (2 to 1000 μm) fatigue cracks in 2090-T8E41 alloy, as a function of the nominal and effective stress intensity ranges, ΔK and ΔK_{eff}, respectively. Data are presented for a) L-T, b) T-L, and (c) T-S orientations at R = 0.1. Note how small crack growth rates exceed those of long cracks by several orders of magnitude when compared on the basis of ΔK, yet show close correspondence when characterized in terms of ΔK_{eff}.

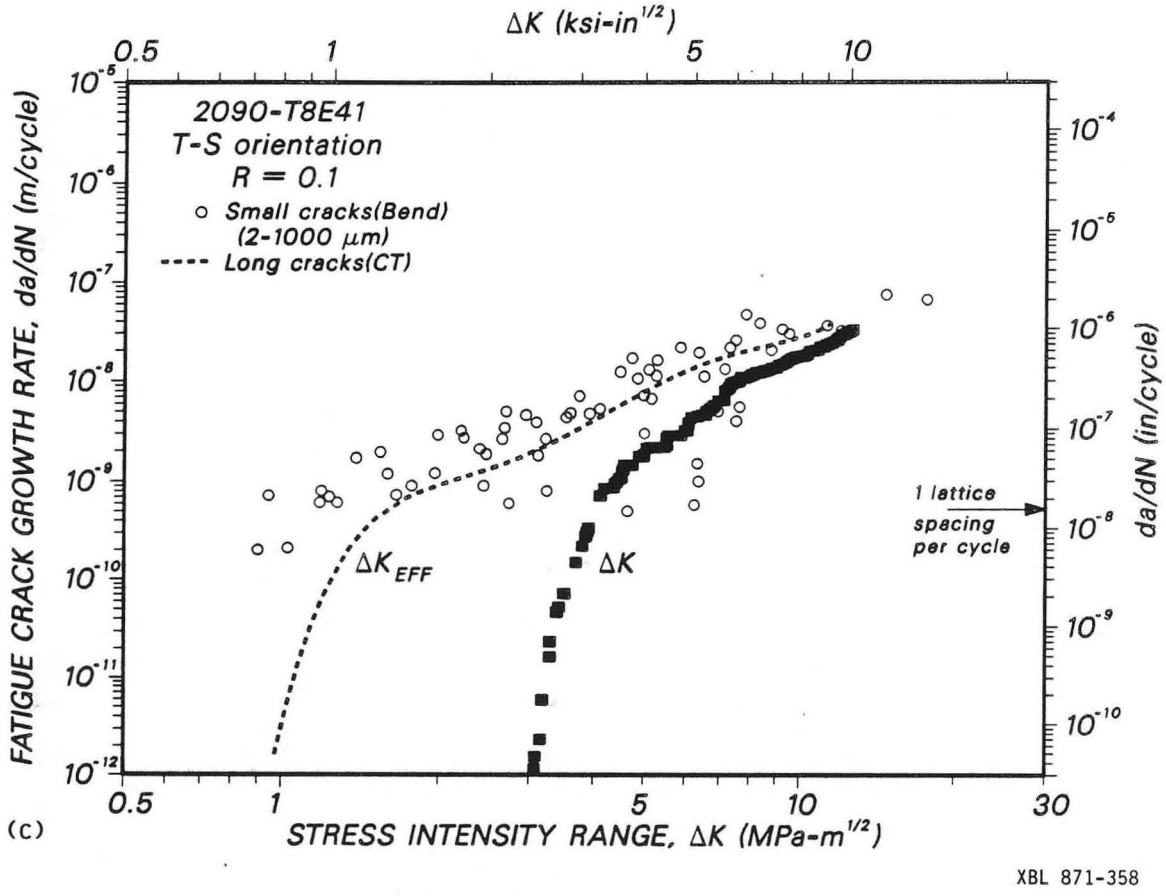
ΔK (ksi-in^1/2)
0.5
1
5
10
2090-T8E41
T-S orientation
R = 0.1
Small cracks(Bend)
(2-1000 μm)
Long cracks(CT)
ΔK_EFF
ΔK
1 lattice spacing per cycle
FATIGUE CRACK GROWTH RATE, da/dN (m/cycle)
da/dN (in/cycle)
STRESS INTENSITY RANGE, ΔK (MPa-m^1/2)
0.5
1
5
10
30
(c)
XBL 871-358

Fig. 7 (Cont.)

LAWRENCE BERKELEY LABORATORY
TECHNICAL INFORMATION DEPARTMENT
UNIVERSITY OF CALIFORNIA
BERKELEY, CALIFORNIA 94720